Unsteady numerical simulation of the flow in the U9 Kaplan turbine model

Ardalan Javadi, Håkan Nilsson

Department of Applied Mechanics, Chalmers University of Technology, Gothenburg, SE-412 96, Sweden

E-mail: ardalan.javadi@chalmers.se

Abstract. The Reynolds-averaged Navier-Stokes equations with the RNG k-ε turbulence model closure are utilized to simulate the unsteady turbulent flow throughout the whole flow passage of the U9 Kaplan turbine model. The U9 Kaplan turbine model comprises 20 stationary guide vanes and 6 rotating blades (700 RPM), working at full load (0.71 m^3/s). The computations are conducted using a general finite volume method, using the OpenFOAM CFD code. A dynamic mesh is used together with a sliding GGI interface to include the effect of the rotating runner. The hub and tip clearances are included in the runner. An analysis is conducted of the unsteady behavior of the flow field, the pressure fluctuation in the draft tube, and the coherent structures of the flow. The tangential and axial velocity distributions at three sections in the draft tube are compared against LDV measurements. The numerical result is in reasonable agreement with the experimental data, and the important flow physics close to the hub in the draft tube is captured. The hub and tip vortices and an on-axis forced vortex are realistically captured. The numerical results show that the frequency of the forced vortex in 1/5 of the runner rotation.

1. Introduction

Hydropower is the longest established source for the generation of electric power, which developed into an industrial size plant following the demonstration of the economic transmission of high-voltage AC. The increasing need for more power during the early years of the twentieth century also led to the invention of a turbine suitable for small heads of water, i.e., 3-9 m, in river locations where a dam could be built. In 1913, Viktor Kaplan revealed his idea of the propeller (or Kaplan) turbine, see Fig. 1, which acts like a ship's propeller but in reverse. At a later date, Kaplan improved his turbine by means of swiveling blades, which improved the efficiency of the turbine appropriate to the available flow rate and head. The Kaplan turbine incorporates the essential feature that the setting of the rnner blade angle can be controlled by a servomechanism to maintain optimum efficiency conditions. This adjustment requires a complementary adjustment of the guide vane angle to maintain an almost swirl-free flow at the exit from the runner.

According to Drtina and Sallaberger [1] and Nilsson [2], the use of computational fluid dynamics (CFD) for predicting the flow in these machines has brought further substantial improvements in their hydraulic design and resulted in a more complete understanding of the flow processes and their influence on the turbine performance. Details of flow separation, loss sources, and loss distributions in components both at design and off-design, as well as detecting low-pressure levels associated with the risk of cavitation, are now amenable to analysis with the aid of CFD. Many investigators have applied

CFD as a numerical simulation tool for the analysis of other turbines [3-7] while there are only a handful profound numerical investigations of the Kaplan turbine. Recently, studies have been performed experimentally and numerically, showing that the low-frequency pressure fluctuation in the draft tube possesses a frequency of 0.15–0.33 times the runner's rotating frequency, and that this pressure fluctuation is mainly induced by the flow at the area near the inlet of the draft tube. Wu *et al.* [8] studied the pressure fluctuations of a prototype Kaplan turbine using RNG k-ε and ended up with close similarity between pressure field in the prototype and the model. Liu *et al.* [9] analyzed pressure fluctuation in a Kaplan turbine draft tube and captured a low frequency vortex rope that rotated in the opposite direction of the runner. Owing to the complexity of the flow field containing, acceleration, deceleration, transition, relaminarization, separation and reattachment, an adequate numerical analysis of such a flow is necessary to help experiment to widen the understanding about the coherent and turbulent structures.

In this paper a model Kaplan turbine is investigated numerically using RNG k-ε at best efficiency point. The full runner passages and guide vanes with all geometrical details are included in the computational domain. The coherent structures, and the instantaneous and periodic features of the flow in the draft tube are discussed. The results show a close agreement with experimental observation and the structures are further clarified. Although the diffusion of the vorticity and the decay of the concentrated vortices possess highly complicated properties and is cumbersome to be captured by time-dependent solutions, the physical properties of the on-axis vorticity pocket is presented.

2. Flow configuration and numerical aspects

The studied test case is the 1:3.1 scale model of the U9 Kaplan turbine prototype. The operational head of the prototype is 55 m with a maximum discharge capacity of 20 m^3/s for a power of 10 MW. The turbine is composed of a spiral casing, 18 stay vanes, 20 guide vanes, 6 runner blades and an elbow draft tube. The prototype runner diameter is 1.55 m. The diameter of the model runner is $D = 0.5$ m, with an operational net head of $H = 7.5$ m, a runner speed of $N = 696.3$, a flow rate is $Q = 0.71$ m^3/s and a guide vane angle of $26°$. The Reynolds number based on draft tube cone is about 1.5×10^7. The present work investigates the turbine at BEP and compares the numerical results with experimental measurement of Mulu [10].

The calculations reported herein are performed using the finite-volume method in the OpenFOAM open source CFD code. The governing equations are the continuity and momentum equations for incompressible flow. The code is parallelized using domain decomposition and the Message Passing Interface (MPI) library. The simulation is performed using an AMD Opteron 6220 Linux cluster and 64 cores. The second-order central difference scheme is used to discretize the diffusion terms, and the second-order linear upwind difference scheme is adopted to approximate the convection term. The time-marching is performed with an implicit second-order accurate backward scheme. The General Grid Interface (GGI) [11] is used at the sliding interfaces between the rotor and the stator. The main advantage of the GGI is that it allows for non-conformal meshes at the interface. It makes mesh generation easier for complex geometries, and facilitates a sliding grid approach. It has been shown to give a close agreement for the velocity results between non-conformal and conformal meshes. However, in the present study it was required to have a proper circumferential mesh resolution on each side of the GGI to yield good results for the turbulent kinetic energy. Nilsson *et al.* [12] validated the use of non-conformal meshes arguing that the spacing should be comparable in the radial and axial direction.

Figure 1 shows the computational domain which includes, the guide vanes (20 blades), the runner (6 blades) and the draft tube. The total number of cells in the domain is 5.7×10^6 where the guide vanes, runner and the draft tube have 2.653×10^6, 1.211×10^6 and 1.847×10^6 cells, respectively. The mesh generation is a challenging task, especially since the geometrical details such as the clearance of the guide vanes, the hub and tip clearance of the runner blades are included in the computational

domain. Figure 1b shows the mesh in the guide vane passage and the runner. A total number of 70 cells with angel smaller than 25 degrees is reported which shows the adequate mesh generation process. The quality of the mesh is a vital element in capturing correct coherent structures, particularly in such a vortex dominated flow.

A constant velocity, yielding the required mass flux, is applied for the velocity at the inlet, and all other boundary conditions are homogenous Neumann. Due to the geometrical complexity, the inlet velocity and the rotational speed are ramped up from very small values to the physical ones. The relaxation factors are also step-wise increased during the simulation to make the solution converge.
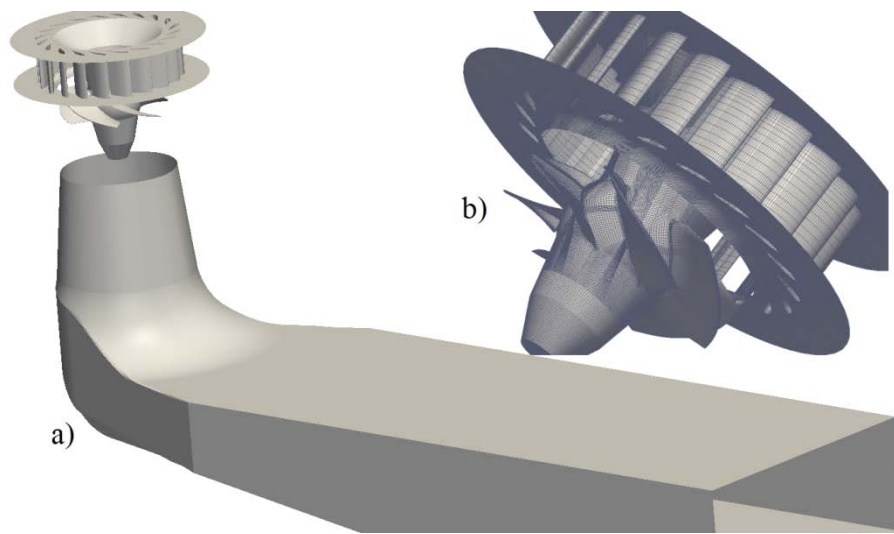
Figure 1. a) computational domain b) mesh in guide vane passage and runner.

3. Results and discussion

The simulation is conducted for more than 25 runner revolutions to established fully periodic flow. The velocity components are averaged for 5 complete runner revolutions. The velocity is normalized by the bulk velocity in the draft tube cone. The survey axis, $S*$ is normalized by the cone radios. Figure 2 shows the mean axial velocity in the draft tube and three survey axis (I, II and III) where the results are extracted. The mean axial velocity contour shows a small recirculation region after the runner cone and along the central low velocity region which is contracted by two high velocity regions. These two high velocity regions are generated by the jet from the hub clearance, (hereafter referred as the hub jet) and expanded downstream.
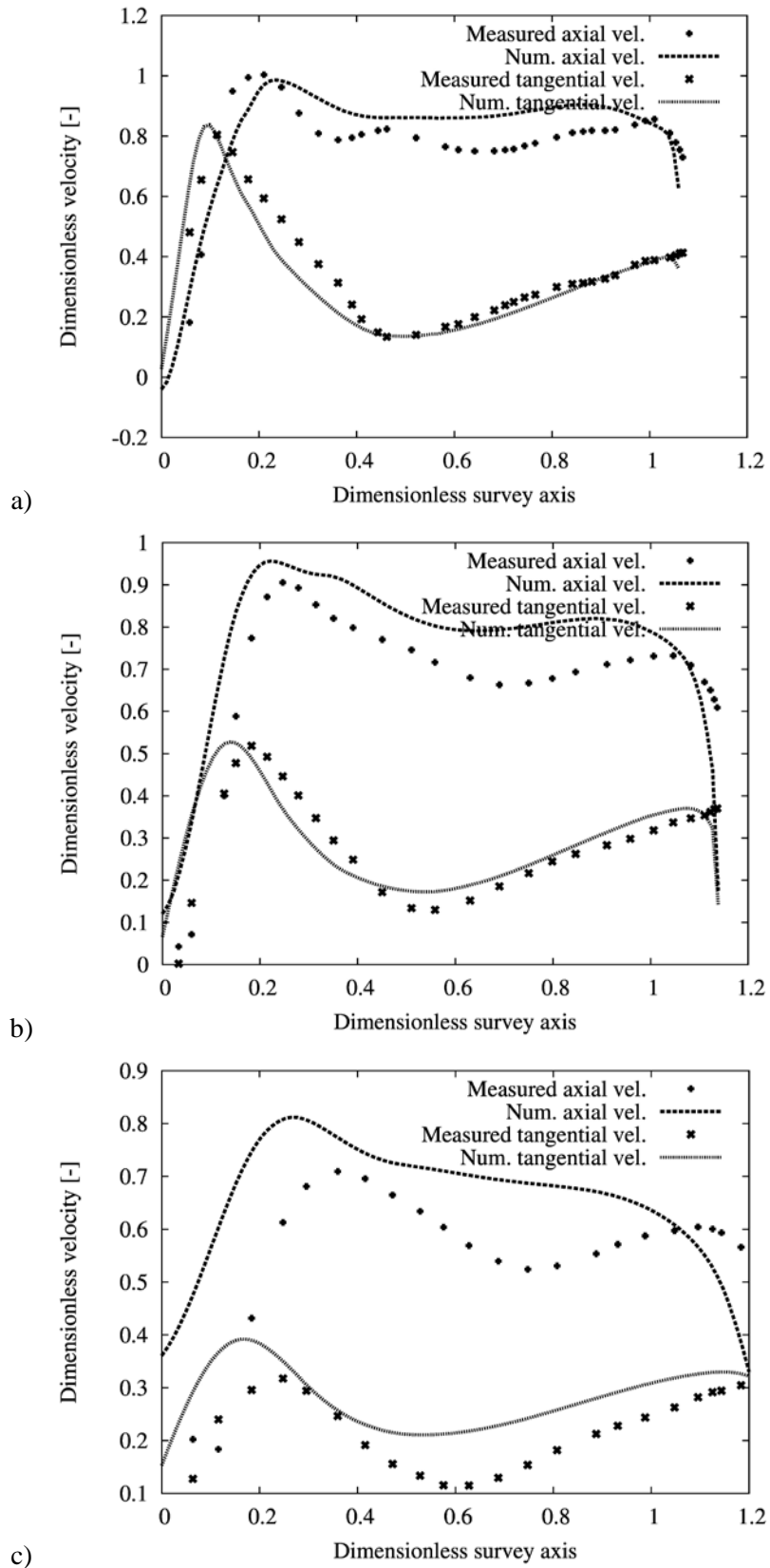
Figure 3 shows the axial and tangential velocity compared with experiment at the three cross-sections, I, II and III, see Fig. 2. The velocity components at cross-section I and II are under high influence of the hub jet. This jet is diffused and less strong at cross-section III. There is an on-axis forced vortex, which is also called as Rankin vortex in the literature. The forced vortex is basically surrounded by a free vortex while in the current flow field the free vortex may not be formed. Nevertheless, the forced vortex is stable for many axial and tangential disturbances, as expected [13]. The linear distribution of the core of the forced vortex, as it can be seen in $S*<0.2$ at cross-section I. The vortex filament is isolated, strong, concentrated and with zero-meridional flow i.e. where the radial and axial velocities are equal to zero. The mid-part of cross-section I, $0.2<S*<0.5$, is dominated by the hub jet which is highly efficient to decrease the swirl in the hub region. Thus, the maximum axial velocity occurs at $S*=0.2$ which can be related to the hub jet. There is a local decrease in the axial velocity which should be related to the hub vortex. This vortex follows the hub jet and the trajectory shows the axial trace of the vortex. The hub jet leads to a linear decrease in the tangential velocity at $0.15<S*<0.3$. This decrease leads to a negative vorticity surrounding the central forced vortex, see Fig. 5. It is worth mentioning that the hub jet generates a strong vortex that is attached to

the with runner cone and finally detaches from the cone. This is the reason behind the hump-like peak of the axial velocity while the tangential velocity is sharp peaked, see Fig. 3a. There is a vortex sheet separating from the trailing edge of the runner blade, traveling downward. This vortex sheet is responsible for the plateau in the axial velocity in $0.5<S^*<1$, see Fig. 3a. The tangential velocity increases linearly in this region which can be related to centrifugal force. Since the detached vortex from the cone and the hub vortex rotate in the opposite direction of the runner and the strong forced vortex, it is being diffused fast. This counter-rotation, see Fig. 5, can be the reason behind the fast dissipation of the tangential velocity in cross-section III, see Fig 3c. The most powerful coherent structure in the flow field is the forced vortex which is twice stronger than the detached vortex from the cone. The forced vortex is highly stable, therefore the detached vortex from the cone can be diffused. According to the numerical results the forced vortex is up to 10 times stronger than the hub vortex, see Fig. 5. Regarding the RANS simulation, the results should be treated with caution, due to the diffusivity of the turbulence model. The simulation captures the tip vortex which cannot be traced far downstream, although there is a sense of tip leakage in the axial velocity at cross-section I. There is weak vortices close to the wall in Fig. 5. The blade tip might be the source of these vortices.

All these flow features are being diffused in the downstream n cross-sections II and III. Since the axial hub jet is powerful enough the forced vortex cannot be diffused radially, therefore the peak of tangential velocity at cross-sections I and II is at $S^* \sim 0.15$. The numerical results are qualitatively correct in the downstream region but overestimate the value of the axial and tangential velocity, which can be related to the quick diffusion of the coherent structures predicted by simulation. In this context, the interaction among the structures decreases and the amount of dissipation decreases yielding an unrealistic amount of dissipation. Thus the simulation overestimates the velocity.


Figure 2. Mean axial velocity [*m/s*] at the center plane. The experimental data is available at cross-sections I, II and III.

a)

b)

c)

Figure 3. Axial and tangential mean velocity compared with experimental results at cross-section a) I b) II c) III.

Figure 4 shows the coherent structures captured by the numerical simulation in the runner and the draft tube. The structures are presented by iso-surface of q-criterion colored by mean pressure. As it can be seen, the pressure decreases from the suction side of the blade which leads to separation of the flow from the blade. The pressure drop continues to the runner cone where minimum pressure occurs. The pressure increases in the downstream, since the swirl decreases and the cross-section of the draft tube increases. The instantaneous pressure which leads to this averaged field is complicated. This complexity yields intertwined and rich flow structures in the runner and the draft tube. The hub clearance is the source of two strong vortices, the former generated at the trailing edge and the latter generated where the blade meets the hub. As it can be seen in Fig. 4, the former is much stronger. Another coherent structure is the tip vortex which generated at the blade tip. The most powerful structure in the draft tube is force vortex, also called Rankin vortex. Another interesting structure which is found in this work is detached hub jet from the runner cone. There is a sudden change of angle in the surface of the runner cone, see Fig. 1, which causes this effects. The detached vortices from the runner cone are the second strongest coherent structure in the field. The tip vortices from the guide vanes are also captured but not reported here.
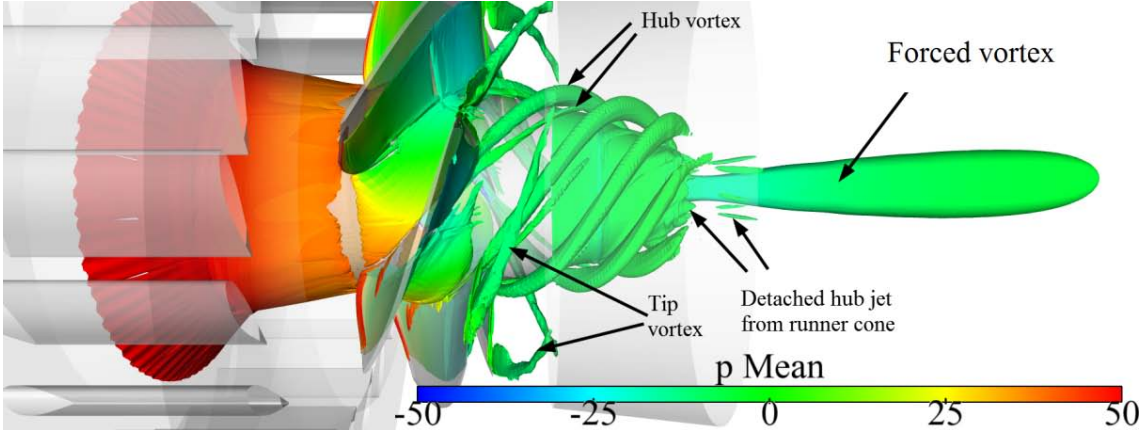
**Figure 4.** Coherent structures in the runner and the draft tube colored by mean pressure [m^2/s^2].
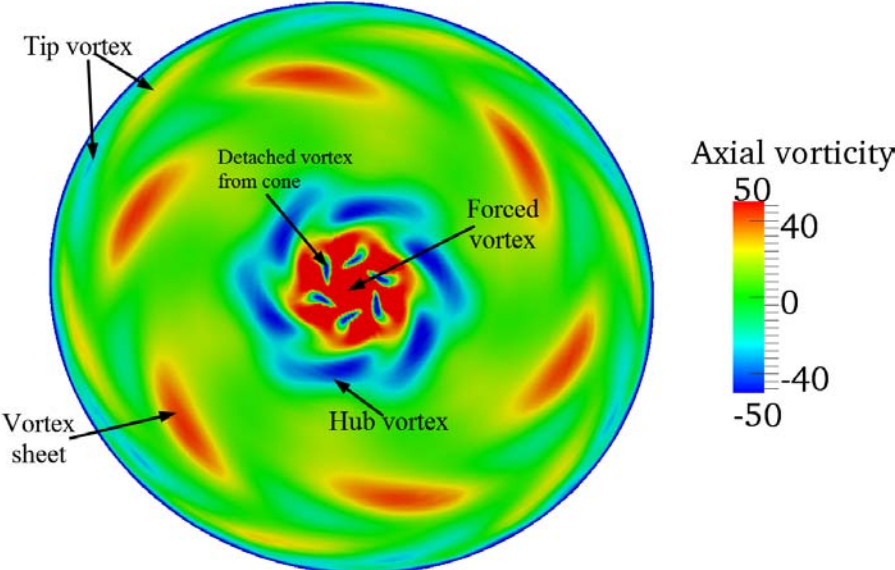
**Figure 5.** Axial vorticity [$1/s$] in a plane close to cross-section I.

Figure 5 shows the axial vorticity at a horizontal cross-section close. The structures are here described from the draft tube wall inwards. The outermost structures related to the tip vortices yielding streaks of positive and negative vorticity. The inner ones should be the vortex sheet separated from the trailing edge of the runner blade. These vortices occupy $0.5<S^*<1$ and are responsible for the plateau in the axial velocity, see Fig. 3. Further inwards, there are counter-rotating hub vortices which surround another counter rotating structure. These vortices are detached from the runner cone. The central forced vortex is surrounded by the detached vortices, dissipates them quickly and will be dissipated in the near downstream. Because diffusive turbulence model is used, these interactions between counter- and co-rotating structures are overestimated. The structures lose their coherence fast, which lead to less downstream interaction. The overestimate of the downstream velocity components in the downstream, Fig. 3, can be related to the diffusivity of the turbulence model. To investigate this issue, advanced numerical simulation of the current test case using hybrid RANS-LES is under way. Javadi and Nilsson [14] investigated various hybrid RANS-LES method in a swirl generator with rotor-stator interaction and confirmed the applicability of the method. Javadi and Nilsson [15] applied a scale-adaptive method for strongly swirling flows. I.e. there are a number of advanced methods to study the current flow field comprehensively.

Figure 6 shows the phase-averaged pressure in a point close to the wall at cross-section I. The horizontal axis is normalized by the runner rotation period. The frequency of the forced vortex is 5 time smaller than the runner rotation which is 5 complete runner frequency. The plot includes 5 revolutions with 30 blades time periods.

Figure 7 shows streamlines in the draft tube colored by instantaneous velocity magnitude. As it can be seen the rate of the swirl is not very high, as expected. The on-axis forced vortex is shifted to the right after the elbow.
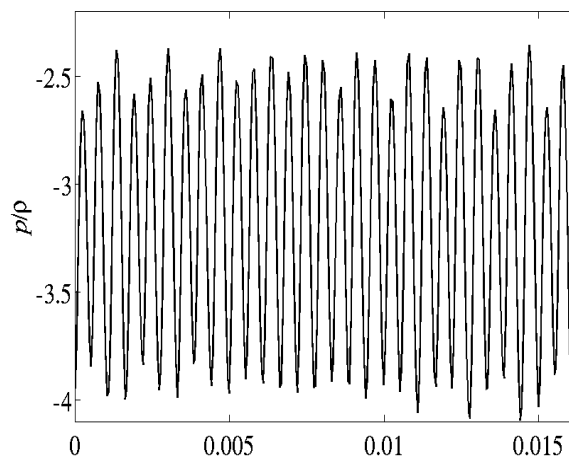
Figure 6. Phase-averaged pressure [m^2/s^2] over one period of the forced vortex.
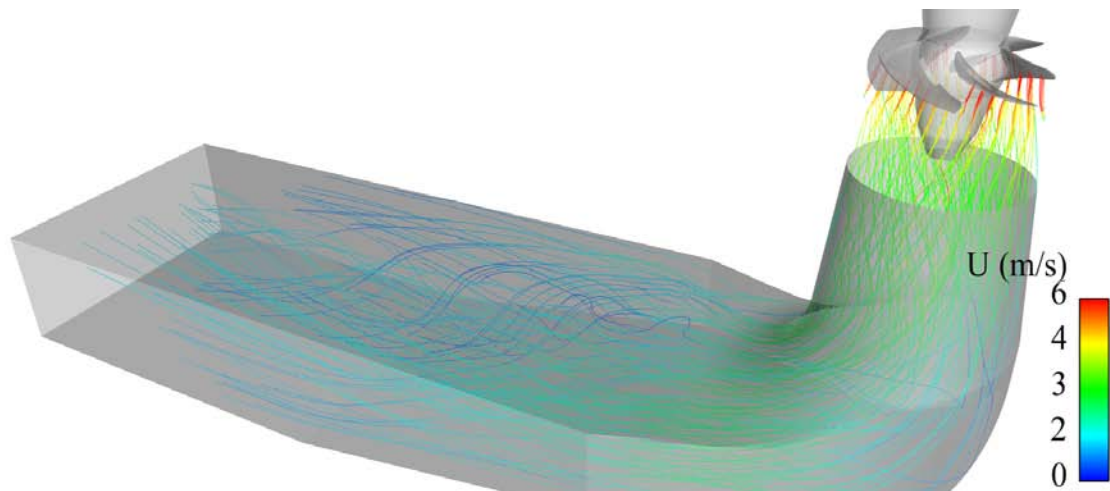
Figure 7. Streamlines in the draft tube colored by instantaneous velocity magnitude [*m/s*].

4. Conclusion

A numerical simulation of the U9 model Kaplan turbine using RNG *k-ε* is presented. The computational domain includes the guide vanes, full runner and the draft tube. The numerical results present reasonable agreement with the measured data. The forced vortex in the draft tube shows the frequency 5 times smaller than the runner frequency. The tip and hub vortices are realistically captured, the qualitative agreement of the average velocity with experiment. Owing to the diffusivity of the numerical modeling, more advanced (hybrid RANS-LES) simulations are underway, first, to verify the validation of current numerical results and second, to clarify the ambiguities about the life cycle of the coherent structures and the effect of geometrical details. To deepen the understanding of this the flow field, the study of the turbulence structures are necessary which is the drawback of RANS model.

References

[1]   Drtina P and Sallaberger M 1999 Hydraulic Turbines-Basic Principles and State-of-the-Art Computational Fluid Dynamics Applications *Proceedings of the Institution of Mechanical Engineers, Part C, 213, 85102*

[2]   Nilsson H 2002 Numerical Investigations of Turbulent Flow in Water Turbines *Ph.D Thesis* (Sweden: Chalmers University of Technology)

[3]   Munten S, Nilsson H and Susan-Resiga R 2009 3D Numerical Analysis of the Unsteady Turbulent Swirling Flow in a Conical Diffuser using Fluent and OpenFOAM, *in Proc. of the 3rd IAHR International Meeting of the Workshop on Cavitation and Dynamic Problems in Hydraulic Machinery and Systems*, (Brno, Czech Republic), 155 – 164.

[4]   Ciocan G, Iliescu M, Vu T C, Nennemann B and Avellan F 2007 Experimental Study and Numerical Simulation of the FLINDT Draft Tube Rotating Vortex *ASME J Fluid Eng*, **129**, 146-158.

[5]   Bosioc A I, Resiga R, Muntean S and Tănasă C 2012 Unsteady Pressure Analysis of a Swirling Flow with Vortex Rope and Axial Water Injection in a Discharge Cone, *ASME J Fluid Eng*,

134(8), 081104, 1-11

[6]   Tănasă C, Resiga R S, Muntean S and Bosioc A 2013 Flow-Feedback Method for Mitigating the Vortex Rope in Decelerated Swirling Flows, *ASME J. Fluids Eng.* **135**(6), 061304, 1-11

[7]   Resiga R, Muntean S, Hasmatuchi V, Anton I and Avellan F 2010 Analysis and Prevention of Vortex Breakdown in the Simplified Discharge Cone of a Francis Turbine *ASME J Fluids Eng,* **132**(5), 051102-15

[8]   Wu Y, Liu S, Dou H, Wu S and Chen T 2012 Numerical Prediction and Similarity Study of Pressure Fluctuation in a Prototype Kaplan Turbine and the Model Turbine, *Computers & Fluids*, **56**(15), 128-142

[9]   Liu S, Li S, and Wu Y 2009 Pressure Fluctuation Prediction of a Model Kaplan Turbine by Unsteady Turbulent Flow Simulation, *ASME J Fluids Eng*, **131**(10),101102-101102-9

[10]   Mulu, B. An experimental and numerical investigation of a Kaplan turbine model, PhD thesis, (Sweden: Lulea University of Technology)

[11]   Beaudoin M and Jasak H 2008 Development of a Generalized Grid Interface for Turbomachinery Simulation with OpenFOAM, *Open source CFD International conference* (Berlin, Germany)

[12]   Nilsson H, Page M, Beaudoin M, Gschaider B and Jasak H 2008 The OpenFOAM turbumachinery working-group and conclusion from the turbomachinery session of the third OpenFOAM workshop, IAHR , *24th symposium on hydraulic machinery and system* (Foz do Iguassu, Brazil)

[13]   Alekseenko V, Kuibin A and Okulov L 2007 Theory of Concentrated Vortices: An Introduction, *Springer*

[14]   Javadi A and Nilsson H 2014 LES and DES of swirling flow with rotor-stator interaction, *in Proc. of the 5th Symposium of Hybrid RANS-LES method* (Texas A&M Univerisity, USA)

[15]   Javadi A and Nilsson H 2014 Comparative study of scale-adaptive and large-eddy simulation of highly swirling turbulent flow through an abrupt expansion, *27th IAHR Symposium on Hydraulic Machinery and Systems* (Montreal, Canada) (*submitted*)